Near-field leakage characterisation of high-pressure CO₂ pipeline

Fujia Liu[1], Yuguo Wu[2,*], Xiaoling Li[3], Ting Li[4]

1.Fujia Liu, Master degree candidate, Email: v587fj@126.com, College of Petroleum Engineering, Liaoning Shihua University, Fushun, China.

2.Yuguo Wu, Professor, Email: ygwu@lnpu.edu.cn, College of Petroleum Engineering, Liaoning Shihua University, Fushun, China.

3.Xiaoling Li, Associate professor, Email: lingzi_1015@163.com, College of Petroleum Engineering, Liaoning Shihua University, Fushun, China.

4.Ting Li, Master degree candidate, Email: 18340385042@163.com, College of Petroleum Engineering, Liaoning Shihua University, Fushun, China.

Abstract

High-pressure CO₂ pipeline transportation is the key of CCS technology, but there is a safety risk of CO₂ leakage, and its near-field multiphase leakage characteristics are less studied at present. In this study, a real gas model based on CFD is constructed, and the Span-Wagner and Peng-Robinson equations are used to calculate the physical properties of CO₂.The Mixture model is adopted, and the gas-liquid phase change is realized by writing a UDF (User-Defined Function). The k-ε and k-ω turbulence models are used to simulate different working conditions, to compare and analyze the leakage characteristics under different conditions, and the influence of leakage aperture on the formation of Mach disk. The simulation results are consistent with the experimental data, and the model reliability is verified. This study is of great significance for understanding the near-field leakage characteristics of high-pressure CO₂ pipelines, and has academic and application value.

Keywords: High-pressure CO₂ piping, leakage behaviour, computational fluid dynamics, phase change model, turbulence model

1. Introduction

In the context of global climate change, a series of environmental problems caused by excessive greenhouse gas emissions have become the focus of extensive attention of the international community, and CO₂, as the most important greenhouse gas, contributes to about 55% of global warming, and its emission reduction is imminent[1]. In order to effectively address this challenge, carbon capture, transportation, storage and utilization (CCUS) technology has emerged as a powerful means to reduce CO₂ emissions and mitigate global

³⁴ warming. This technology realizes large-scale CO_2 emission reduction by separating CO_2

³⁵ produced by industry, energy and other industries, and transporting it to the seabed or

³⁶ underground where it is isolated from the atmosphere [2].

³⁷   In the CCUS technology chain, pipeline transportation has become the preferred method

³⁸ for large-scale, long-distance, and low-cost transportation of CO_2 on land by virtue of its

³⁹ significant advantages in terms of transportation scale, cost, and social benefits[3]. With the

⁴⁰ growth of global demand for CCUS technology, the construction scale of high-pressure CO_2

⁴¹ pipelines is also gradually expanding.

⁴²   However, with the gradual expansion of the construction scale of high-pressure CO_2

⁴³ pipelines, its potential risk of leakage should not be ignored. Unlike natural gas and other

⁴⁴ conventional transportation media, high-pressure CO_2 will cause serious harm if it leaks. When

⁴⁵ high-pressure CO_2 leaks from the pipeline into the air, due to the Joule - Thompson effect, its

⁴⁶ temperature will drop dramatically, and can even fall below the CO_2 three-phase point to form

⁴⁷ dry ice. This great temperature difference with the surrounding environment will lead to violent

⁴⁸ boiling and evaporation of the leaked CO_2, absorbing a lot of heat from the environment,

⁴⁹ resulting in a sudden drop in the ambient temperature, causing frostbite threat to nearby people

⁵⁰ and animals. At the same time, CO_2 itself belongs to the asphyxiating gas, when the

⁵¹ concentration of CO_2 in the air exceeds 7%, it may lead to unconsciousness or even death. After

⁵² a pipeline leak, CO_2, which is denser than air, will gather in the near-surface area near the

⁵³ leakage port, forming a large, highly concentrated gas cloud and spreading with the

⁵⁴ atmospheric drift, posing a serious asphyxiation risk to people who are too late to evacuate. In

⁵⁵ addition, if the low-temperature CO_2 leaks into water, the mixing of two liquids with great

⁵⁶ temperature differences may trigger a rapid phase change reaction, causing the superheated

⁵⁷ liquid to boil instantaneously, generating an overpressure similar to the effect of an explosion,

⁵⁸ and seriously damaging the structures and equipment near the leak[4].

⁵⁹   In view of the above, it is of great practical significance to study in depth the near-field

⁶⁰ leakage characteristics of high-pressure CO_2 pipelines. However, the existing studies are still

⁶¹ insufficient to explore the near-field multiphase diffusion characteristics, and have not yet

⁶² formed a perfect specification and system applicable to CO_2 pipeline leakage. Therefore,

⁶³ strengthening the research in this area and analyzing the near-field multiphase diffusion

⁶⁴ characteristics are of decisive importance for optimizing the safety assessment of CO_2 pipelines

⁶⁵ and formulating the corresponding protective measures, which will also contribute to the

⁶⁶ advancement of CCS technology and the reduction of global carbon emissions.

67　　　　Many studies have been conducted to address the leakage of CO_2 from high-pressure

68　　pipelines:

69　　　　In 2014, Liu et al.[5] calculated the physical properties of single-phase CO_2 jet using the

70　　user-defined gas phase model in ANSYS FLUENT, without involving multiphase flow of

71　　supercritical CO_2 leakage. In 2016, Zheng et al[6]. established a two-phase flow model for

72　　liquid CO_2 leakage, considering real gas effects, but its effectiveness remained to be verified

73　　by experiments. In 2017, Diana Schumann's team[7] conducted a public perception survey on

74　　CO_2 pipelines in Germany, indicating that public opinions should be considered in site

75　　selection. In 2019, Li Kang et al[8]. numerically simulated the near-field underexpanded jet of

76　　high-pressure CO_2 leakage, and the results were in good agreement with experiments. In 2020,

77　　Lin Teng et al.[9] studied the multiphase flow characteristics of near-field CO_2 jet using

78　　compressible multiphase flow CFD combined with a non-equilibrium phase change model and

79　　verified the results. In 2021, Tian Genyuan's team[10] experimentally observed the pressure

80　　response and phase change during high-pressure CO_2 leakage, finding that different initial

81　　states led to different decompression processes, and low temperature did not damage materials.

82　　In 2022, Hu Yanwei et al[11]. predicted the leakage hazard zones of high-pressure CO_2

83　　pipelines with different diameters, and quantitatively analyzed the relationship between

84　　diameter and hazard distance. In 2023, Chen Junwen et al.[12] studied the rupture leakage of

85　　supercritical CO_2 pipelines, explored safety thresholds using PHAST simulation, and found

86　　that 4% molar concentration was more suitable for evaluating the leakage range. The impact

87　　of CO_2 pipeline leakage was greater than that of natural gas pipelines, significantly affected by

88　　pipe length and outer diameter, but insensitive to pressure. In the same year, Li Zilun[13]

89　　studied the safety of high-pressure CO_2 pipelines, modeled and found that flow velocity and

90　　impurities dominated the decompression of upstream and downstream during pipeline rupture,

91　　and external diffusion was affected by multiple factors. In 2024, Zhang Zixuan et al[14].

92　　discussed the hazards of high-pressure CO_2 leakage accidents to improve the accuracy of

93　　transient release prediction; Wang Jun et al.[15]carried out full-scale blasting tests and

94　　numerical simulations on the failure consequences of high-pressure CO_2 pipelines, built an

95　　82.7-meter buried pipeline test section, measured the downwind CO_2 concentration and

96　　temperature after detonating the middle with explosives, and predicted the failure consequence

97　　distances of different pipeline sizes under different wind speeds with CFD models to provide a

98　　basis for pipeline risk assessment; Sun Jingze[16] simulated supercritical/dense-phase CO_2

99　　leakage with OLGA, compared simulation and experimental values, analyzed the influence of

100　　initial conditions and leakage aperture, and concluded that the software results were

101 conservative and applicable; Luo Zhenmin et al.[17] established a source model considering

102 dry ice formation, simulated liquid CO_2 jet diffusion with CFD and verified it by experiments,

103 studying the influence of factors on parameters and hazard distance, with small prediction

104 errors in the model, and the hazard distance was greatly affected by source intensity, etc.; Yan

105 Shang et al.[18]proposed a new model for predicting the near-field leakage characteristics of

106 high-pressure CO_2 pipelines in 2024, analyzed the influence of initial parameters, and gave a

107 prediction formula for Mach disk characteristics with a maximum error rate of 5.5%; in the

108 same year, Jiaqiang Wang et al. [19]conducted experiments on the near-field characteristics of

109 high-pressure CO_2 pipeline leakage, built a 3000mm-long stainless steel pipeline device,

110 measured near-field temperature, pressure, and jet structure through four aperture sizes (5-

111 40mm) under different initial pressures (4.12-13.16MPa) and temperatures (282.56-334.55K),

112 and analyzed the influence of initial parameters and aperture to provide data for leakage risk

113 assessment. In 2025, Sun Yuan et al.[20] experimentally and numerically simulated the leakage

114 and diffusion of underwater gas pipelines, established a system to analyze influencing factors,

115 built and verified a model based on the Euler-Lagrangian method, and concluded the three

116 stages of leakage diffusion, with acceptable prediction errors in the model.

117 To date, the near-field leakage characteristics of high-pressure CO_2 pipelines have been

118 extensively studied through experimental methods. However, numerical simulations in this

119 area remain insufficient and lack depth. A significant challenge lies in capturing the leakage

120 rate within the first few milliseconds of a high-pressure CO_2 pipeline leak, as the rapid pressure

121 drop during this phase complicates measurements. This difficulty is further exacerbated when

122 considering varying leakage environments, making numerical simulation studies in this domain

123 particularly scarce.To address this gap, this study develops an innovative Computational Fluid

124 Dynamics (CFD) model that integrates the Peng-Robinson equation of state (P-R EOS) for

125 gaseous CO_2 and the Span-Wagner equation of state (S-W EOS) for liquid CO_2. The simulation

126 results generated by this model demonstrate strong agreement with available experimental data,

127 validating its reliability. Leveraging this model, the near-field leakage characteristics of high-

128 pressure CO_2 pipelines are thoroughly investigated.A key focus of this study is the systematic

129 analysis of near-field leakage velocity. By visualizing the formation process of the velocity

130 Mach disk under different operating conditions, the study provides clear, time-scaled cloud

131 diagrams to illustrate this phenomenon. Additionally, recognizing that high-pressure CO_2

132 pipelines often traverse geographically sensitive areas such as lakes and rivers, this study

133 conducts a comprehensive comparative analysis of leakage behavior in different environments.

۱۳۴ The findings offer a scientific basis for optimizing the layout and safety assessment of high-

۱۳۵ pressure CO_2 pipelines in diverse geographic settings.

2. Research Methodology

۱۳۷ The computational fluid dynamics (CFD) model used in this study is mainly based on a

۱۳۸ multiphase flow model, a turbulence model, and a physical property calculation method

۱۳۹ incorporating the Peng-Robinson equation of state (P-R EOS) and the Span-Wagner equation

۱٤۰ of state (S-W EOS). It is considered that the pressure drop time in the near-field leakage

۱٤۱ scenario is extremely short, which triggers the phenomenon of a drastic phase transition of CO_2

۱٤۲ and is accompanied by the appearance of Thomson throttling effect. Based on this background,

۱٤۳ the accurate fitting of the phase change model, the turbulence model, and the CO_2 physical

۱٤٤ property equation during numerical simulations is particularly critical. However, there is

۱٤٥ currently a lack of a well-developed theoretical framework to elucidate and characterize the

۱٤٦ principles of dry ice formation under conditions below the three-phase point. Therefore, in

۱٤۷ order to simplify the research methodology, this study reduces the phase change process of CO_2

۱٤۸ to gas-liquid phase transformation. Specifically, solid, liquid, and supercritical CO_2 are

۱٤۹ collectively regarded as the primary phase, while gaseous CO_2 and air are grouped into the

۱٥۰ secondary phase. Additionally, air is assumed to behave as an ideal gas, and gravitational

۱٥۱ effects are neglected. This model, although effectively reducing computational complexity, is

۱٥۲ only applicable for studying the jet characteristics in the near-leakage field over a short time

۱٥۳ span. In terms of simulation, a transient approach is adopted, and the PISO algorithm is

۱٥٤ employed as the solution strategy to capture the dynamic changes during the leakage process.

۱٥٥ *2.1. Governing equation*

۱٥٦ To predict the source intensity of supercritical CO_2 leakage, a compressible multiphase

۱٥۷ flow model is required to solve the continuity equation, momentum equation, and energy

۱٥۸ equation. As shown in Equations 1-3, this model can describe the compressible flow of CO_2 in

۱٥۹ all its phases as well as air.

۱٦۰
$$\frac{\partial \bar{\rho}}{\partial t} + \frac{\partial}{\partial x_i}\left(\bar{\rho}\bar{u}_i\right) = 0 \tag{1}$$

۱٦۱
$$\frac{\partial}{\partial t}(\bar{\rho}\bar{u}_i) + \frac{\partial}{\partial x_i}(\bar{\rho}\bar{u}_i\bar{u}_j) = -\frac{\partial \bar{p}}{\partial x_i} + \frac{\partial}{\partial x_i}(\bar{\rho}\overline{u_i'u_j'}) + S_u \tag{2}$$

۱٦۲
$$\frac{\partial \bar{E}}{\partial t} + \frac{\partial}{\partial x_i}\left[\left(\bar{E}+\bar{p}\right)\bar{u}_i - \overline{u_i'u_i'u_j'}\right] = \frac{\partial}{\partial x_i}\left(\lambda\frac{\partial \bar{T}}{\partial x_i}\right) + S_E \tag{3}$$

2.2. Multiphase flow modeling

١٦٤   During high-pressure CO_2 leakage, the interaction between the gas phase involved and the

١٦٥   liquid phase that may be formed (e.g., some CO_2 will liquefy under certain pressure and

١٦٦   temperature conditions) is extremely critical. Different multiphase flow models are available

١٦٧   for different phase distributions and flow regimes. Only by choosing the right model can we

١٦٨   accurately simulate the core physical characteristics such as phase change, velocity

١٦٩   distribution, temperature distribution, etc. of a high-pressure CO_2 leakage, and then ensure that

١٧٠   the simulation results are in good agreement with the actual leakage situation. In FLUENT2023

١٧١   software, three multiphase flow models are provided for researchers to choose fro[21]: DPM,

١٧٢   VOF and Mixture models. DPM is suitable for scenarios in which the particle volume does not

١٧٣   account for more than 10% of the total volume; VOF is good at describing the interfacial

١٧٤   characteristics of multiphase flow and is suitable for unsteady flow; and Mixture takes into

١٧٥   account the velocity differences and interactions between the discrete phase and the continuous

١٧٦   phase. For the gas-liquid phase change problem of CO_2, a clear interface between the two

١٧٧   phases after the phase change of CO_2 cannot be clearly delineated. In addition, this study did

١٧٨   not deal with the problem of solid-state CO_2, so the Mixture model was chosen to be used. And

١٧٩   the code for the mass source term was handled by writing a UDF in order to realize the phase

١٨٠   transition process. Meanwhile, the pressure-temperature gas-liquid saturation line was

١٨١   generated according to the Span-Wagner equation of state (S-W EOS). In detail, the increase

١٨٢   or decrease of gas-liquid mass is controlled by the following equation to realize the gas-liquid

١٨٣   phase change[22]:

١٨٤
$$If\ (p < p_{sat}):$$

١٨٥
$$m = c\alpha_l \rho_l \frac{p_{sat} - p_l}{p_{sat}} \tag{4}$$

١٨٦
$$If\ (p > p_{sat}):$$

١٨٧
$$m = -c\alpha_g \rho_g \frac{p_{sat} - p_g}{p_{sat}} \tag{5}$$

١٨٨   **Where: c is the phase transition rate coefficient. α is the volume fraction and ρ is**

١٨٩   **the density.**

١٩٠   After obtaining the mass source term, the energy source term produced by the phase

١٩١   transition is:

١٩٢
$$S = H^* m \tag{6}$$

١٩٣   **Where: H is the latent heat of vaporization at the specified temperature.**

١٩٤   *2.3. Turbulence Modelling*

١٩٥   Thanks to the efforts of many scholars, a variety of turbulence models have been

١٩٦   developed, including some widely known models such as the k-ε realizable model and the k-ω

١٩٧   SST (shear stress transport) model. In order to accurately predict the flow phenomena near the

١٩٨   leakage point of a CO_2 pipeline, it is particularly important to deeply investigate the under-

١٩٩   expansion jets formed by the high-pressure gas release. Considering that the under-expanded

٢٠٠   flow involves both turbulent mixing and compression effects, it becomes a crucial issue to

٢٠١   evaluate whether the selected turbulence model can effectively map these critical effects.

٢٠٢   For further understanding and investigation, six numerical simulation experiments were

٢٠٣   conducted in this paper. In these experiments, a fixed temperature (269.65 K) and pressure

٢٠٤   (4.05 MPa) were set, different leakage apertures (4 mm, 20 mm, and 40 mm) were selected,

٢٠٥   and two turbulence models: the k - ε model and the k - ω model, were used to perform the

٢٠٦   corresponding simulation experiments. Through the analysis and comparison (as shown in

٢٠٧   Table 1), it is found that the k - ω SST (shear stress transport) model can provide better

٢٠٨   simulation results when the leakage aperture is small; on the contrary, the k - ε model shows

٢٠٩   better simulation performance when the leakage aperture is large.This is because the k-ω model

٢١٠   exhibits superior predictive accuracy for small-diameter leaks (laminar-turbulent transition

٢١١   zone), whereas the k-ε model is more suitable for large-diameter turbulent-dominated leakage

٢١٢   scenarios. This conclusion stems from the fundamental theory of fluid mechanics: the boundary

٢١٣   layer effect is significant under small apertures, necessitating the capture of near-wall flow

٢١٤   characteristics through the shear stress transmission mechanism of the k-ω model; in large-

٢١٥   diameter leaks, the k-ε model's global description of the turbulent dissipation rate better aligns

٢١٦   with fully developed turbulent flow fields. The flow field characteristics presented in the

٢١٧   velocity contour plot in Table 2, specifically whether there is a sharp velocity decay

٢١٨   downstream of the Mach disk formation region to a near-zero value in the form of a blue

٢١٩   triangular low-velocity zone, can serve as a key basis for verifying the applicability of the two

٢٢٠   models.

٢٢١   *2.4. Fitting of physical property equations for CO_2*

٢٢٢   First of all, liquid CO_2 and gaseous CO_2 need to be treated as two separate fluids when

٢٢٣   simulation calculations are performed using FLUENT software. Only in this way can the

٢٢٤   FLUENT simulation software accurately differentiate between the liquid and gas states when

٢٢٥   the phase transition phenomenon occurs, and thus accurately simulate the phase transition

٢٢٦   process. In addition, in the process of phase change calculation, the influence of the spinning

۲۲۷ knot line must be considered. That is, in the actual phase transition process, there will be the
۲۲۸ phenomenon of superheated liquid fluid and supercooled gaseous fluid (the specific region is
۲۲۹ shown in Fig. 1), which can be interpreted as the incompleteness of the phase transition process.
۲۳۰ Therefore, in the vicinity of the saturation line, the physical properties of the liquid and gaseous
۲۳۱ states need to be extended.

۲۳۲ Secondly, a large number of researchers and scholars have adopted the Peng-Robinson
۲۳۳ equation of state (P-R EOS)[23] to calculate the thermodynamic parameters of CO_2, and this
۲۳٤ method has shown relatively excellent accuracy in modeling the leakage process. However, a
۲۳۵ study by Flechas T et al. [24] compared in depth the performance of both Peng-Robinson
۲۳٦ equation of state (P-R EOS) and Span-Wagner equation of state (S-W EOS) for the prediction
۲۳۷ of CO_2 physical properties, revealing that the latter exhibits a higher degree of accuracy only
۲۳۸ close to the critical point.

۲۳۹ Therefore, the physical properties of liquid CO_2 in this study, including parameters such
۲٤۰ as density, thermal conductivity, viscosity, specific heat capacity, and speed of sound, were
۲٤۱ obtained by writing a UDRGM （User Defined Real Gas Model）and using the bilinear
۲٤۲ interpolation method (the principle of bilinear interpolation is shown in Fig. 2, in which the
۲٤۳ horizontal and vertical axes of the physical properties table represent uniformly spaced
۲٤٤ temperature and pressure values, respectively. After calculation, a series of points similar to
۲٤۵ Q11, Q12, Q21, and Q22 can be obtained, and then the value corresponding to point P is
۲٤٦ calculated according to Eqs. 7-9. (In other words, the value of any point in the table range can
۲٤۷ be derived from calculations based on the values of the four known points around it.) Obtained
۲٤۸ from physical property data extracted from the REFPROP database . It is worth noting that the
۲٤۹ physical property data in this database were calculated based on Span-Wagner[25]equation of
۲۵۰ state (S-W EOS). Therefore, it can be assumed that the work of fitting the physical properties
۲۵۱ of liquid CO_2 in this study was based on the Span-Wagner equation of state (S-W EOS).

۲۵۲ In order to ensure the stability of the calculation process, the Peng-Robinson (P-R EOS)
۲۵۳ equation of state built-in FLUENT software was used to calculate the density data of gaseous
۲۵٤ CO_2 in this study. Meanwhile, the data were read from the physical property data table by
۲۵۵ writing a UDF and combining it with a bilinear interpolation method in order to obtain the
۲۵٦ physical property parameters such as viscosity, thermal conductivity and specific heat capacity.
۲۵۷ Specifically, the simulation of physical parameters for gaseous CO_2 in this study is based on
۲۵۸ the Peng-Robinson equation of state (P-R EOS), while the simulation of physical parameters

٢٥٩   for liquid CO_2 is based on the Span-Wagner equation of state (S-W EOS). Peng-Robinson

٢٦٠   equation of state (P-R EOS) is shown below:

$$f\left(R_1\right) \approx \frac{x_2 - x}{x_2 - x_1} f\left(Q_{11}\right) + \frac{x - x_1}{x_2 - x_1} f\left(Q_{21}\right) \tag{7}$$

$$f\left(R_2\right) \approx \frac{x_2 - x}{x_2 - x_1} f\left(Q_{12}\right) + \frac{x - x_1}{x_2 - x_1} f\left(Q_{22}\right) \tag{8}$$

$$f\left(P\right) \approx \frac{y_2 - y}{y_2 - y_1} f\left(R_1\right) + \frac{y - y_1}{y_2 - y_1} f\left(R_2\right) \tag{9}$$

$$P = \frac{R_g T}{v - b} - \frac{a}{v^2 + 2bv - b^2} \tag{10}$$

$$a = 0.45724 \cdot \frac{R_g^2 T_c^2}{P_c} \cdot \alpha\left(T, \omega\right) \tag{11}$$

$$b = 0.07780 \cdot \frac{R_g T_c}{P_c} \tag{12}$$

$$\alpha\left(T, \omega\right) = \left[1 + \left(0.37464 + 1.54226\omega - 0.26992\omega^2\right)\left(1 - \sqrt{\frac{T}{T_c}}\right)\right]^2 \tag{13}$$

٢٦٨   **Where Tc, Pc are the critical points of temperature and pressure, respectively. For**

٢٦٩   **CO2, ω = 0.224.**

٢٧٠   Considering that the specific heat function defined in the UDF can only be read based on

٢٧١   the change of temperature, the specific heat of gaseous CO_2 at was treated in this study by

٢٧٢   fitting the temperature values on the gas-liquid P-T saturation line for the part below the critical

٢٧٣   point. While for the part above the critical point, the fitting was done based on the Wilton line

٢٧٤   equation (as shown in Eq. 14).

$$\ln\left(P_r\right) = -7.518 + \frac{7.528}{T} + 15.189 \times \ln\left(T_r\right) \tag{14}$$

٢٧٦   **Where: Pr and Tr are the critical pressure and temperature, respectively.**

٢٧٧   *2.5. Principles of Mach disc Formation*

٢٧٨   When the static pressure at the nozzle outlet reaches or exceeds twice the static pressure

٢٧٩   of the surrounding medium, a supersonic highly under expanded jet is formed. At this point,

٢٨٠   the static pressure at the nozzle outlet does not match the ambient pressure, and a Prandtl Meyer

٢٨١   expansion wave is generated in the jet, causing the gas to accelerate and the pressure to

٢٨٢   decrease. Expansion waves reflect and converge to form compression waves, and when the

٢٨٣   static pressure at the outlet is high, interception shock waves are formed. When the airflow

284 passes through the interception shock wave, it will be compressed again. When the height is
285 under expanded, the jet core still cannot make the pressure consistent with the ambient
286 pressure. Therefore, a Mach disk is formed on the centerline of the jet, inducing the reflection
287 of oblique shock waves and forming a "Mach disk three wave co-intersection" structure. As
288 shown in Figure 3.

289 **3. Content of the study**

290 *3.1*. Experimental process

291 Pursell [26]conducted jet release experiments on saturated gaseous or liquid CO_2 in the
292 Health and Safety Laboratory using an apparatus consisting of, among other things, a 60 L
293 jacketed pressurized feed vessel (see Figure 4). The experiments were conducted at an initial
294 pressure of 40 - 55 bar, focusing on four conditions: release orifice diameter of 2 mm or 4 mm,
295 and supply phase in saturated gaseous or liquid state. Experimental measurements were taken
296 to record key parameters such as temperature, and one of the experimental conditions was:
297 initial pressure of 4.05 Mpa in the pipeline, initial temperature of 269.65 K, leakage orifice
298 diameter of 4 mm, and external ambient pressure of 101325 Pa and temperature of 290 K. A
299 two-dimensional model was constructed based on this condition in this study in order to
300 validate the reliability of the computational hydrodynamics model from the point of view of
301 the structure of the leakage jets.

302 Wareing et al [27] experimented in a large laboratory vessel equipped with a separate
303 ventilation system. A 20 mL tank of liquid CO_2 was pressurized to 68.9 bar equilibrium for 1 h
304 and then fixed, and CO_2 was released through a 0.5 mm or 1.0 mm customized nozzle into a
305 special Plexiglas box . Measurements were taken at different locations on the jet centerline
306 using a Dantec fiberflow laser Doppler anemometer (LDA). The experiments simulated the
307 actual emission, and the data processing revealed that: the initial particle distribution after
308 Mach surge is independent of the nozzle size; there is agglomeration in the 1.0-mm-diameter
309 nozzle jet, but not in the 0.5-mm one; the particles are close to the velocity equilibrium at 50
310 mm from the nozzle; and the diffusion angle of particle velocity vectors is more pronounced in
311 the 1.0-mm-diameter nozzle jet as the distance increases. In this study, a two-dimensional
312 model is constructed based on this 1 mm leakage diameter condition to verify the reliability of
313 the computational fluid dynamics model from the perspective of leakage velocity.

314 *3.2. Modelling and meshing*

۳۱۵   In this study, a two-dimensional model was constructed as shown in Fig. 5. During the
۳۱٦ calculation process, this 2D model is rotated 360 degrees according to the rotation axis shown
۳۱۷ in the figure to match the actual leakage situation. Specifically:

۳۱۸   (1) The boundary condition of ac is set as an axisymmetric condition;

۳۱۹   (2) The boundary conditions for ag and gf are set to wall conditions;

۳۲۰   (3) The boundary conditions for ed, dc, and ef are set to pressure exit conditions;

۳۲۱   (4) fb serves as a leakage port and its boundary conditions are set as internal conditions;

۳۲۲   (5) abfg indicates the pipeline area;

۳۲۳   (6) edcbf indicates the area of leakage.

۳۲٤   In this study, for the meshing needs, only the regions where phase transition phenomena
۳۲۵ occur need to be densified, while the non-phase transition regions do not need to refine the
۳۲٦ mesh. Accordingly, adaptive meshing technique is selected as the meshing method for
۳۲۷ numerical simulation in this study.

۳۲۸   The specific steps are as follows: the preliminary step is to perform a uniform meshing as
۳۲۹ demonstrated in Figure 6. Subsequently, the relevant regions are labeled in the FLUENT
۳۳۰ software and the adaptive mesh function is activated. Next, the parameters are set so that the
۳۳۱ system will automatically perform the encrypted grid division when the grid volume occupied
۳۳۲ by gaseous CO_2 due to phase transition exceeds 10% of the total grid volume. By this method,
۳۳۳ not only the time required for calculation is significantly reduced, but also the accuracy of the
۳۳٤ calculation process is ensured.This article conducts speed comparison experiments under the
۳۳۵ working conditions of initial pressure of 12 MPa, temperature of 280 K, and leakage diameter
۳۳٦ of 40 mm, with parameters set at 1%, 5%, 10%, 30%, and 80%, respectively. The number of
۳۳۷ computational grids obtained from the experiments is 71,392, 65,968, 63,142, 57,496, and
۳۳۸ 48,763, respectively. The results indicate that the speed curve exhibits significant deviations
۳۳۹ when the parameter value is 80%, while the speed curves under the other parameters align well.
۳٤۰ Based on this, grid independence verification is completed, and the 63,142 grids corresponding
۳٤۱ to the parameter of 10% are ultimately selected as the simulation computational grid, as shown
۳٤۲ in Figure 7.

۳٤۳   *3.3. Numerical simulation experiment and result analysis*

۳٤٤   In this study, Experiment I and Experiment VIII were first conducted and mutually
۳٤۵ verified with related experiments. On this basis, eight numerical simulation experiments were
۳٤٦ conducted to analyze in detail the leakage near-field characteristics of high-pressure CO_2
۳٤۷ pipelines under different leakage apertures, initial pressures, and leakage environments.

٣٤٨   3.3.1 Validation of the model and description of the working conditions

٣٤٩   According to the relevant experimental [26]settings, where the working conditions include

٣٥٠   an initial pressure of 4.05 MPa, an initial temperature of 269.65 K and a leakage aperture of 4

٣٥١   mm, the experimental data under these conditions are compared with the numerically simulated

٣٥٢   velocity cloud from Experiment 1 of the present study, and the results of the comparison are

٣٥٣   shown in Fig.8.It is evident from the figure that the structural consistency between the two is

٣٥٤   high, and the relative errors in the length of the expansion zone and the effective diameter are

٣٥٥   4.3 mm and 3.9 mm, respectively, with relatively small absolute values of error. This further

٣٥٦   verifies the accuracy of the model used in this study, laying a solid foundation for subsequent

٣٥٧   research.

٣٥٨   Figure 9 illustrates the results of the velocity simulation modelling for Experiment VIII

٣٥٩   compared to the validation of the experimental data. The experimental data are derived from

٣٦٠   the small-scale experiment of Wareing et all[27] which has an initial pressure of 6.89 MPa and

٣٦١   a leakage aperture of 1 mm. the same working conditions are used in Experiment VIII. As can

٣٦٢   be seen from the figure, the overall simulation results fit well with the actual data. However,

٣٦٣   the maximum velocity in the simulation results is slightly lower than the actual data, which

٣٦٤   may be due to the generation of dry ice particles in the experiment and the simplification of the

٣٦٥   dry ice generation process in this study, which leads to a certain error. In addition, due to the

٣٦٦   small leakage aperture, there is still a sudden change in velocity although Mach disk does not

٣٦٧   appear, which is also consistent with the aerodynamic theory.

٣٦٨   After successfully verifying the accuracy of the model through two experiments, in terms

٣٦٩   of both jet structure and leakage velocity, this study continued with eight simulation

٣٧٠   experiments.The specific conditions of each experiment are listed in Table 2, in order to clearly

٣٧١   and intuitively show the working conditions under different conditions, thus providing a clear

٣٧٢   basis and reference for the subsequent in-depth analysis of the numerical simulation results.

٣٧٣   *3.3.2 Analysis of the impact of leakage aperture*

٣٧٤   It is of great significance to study the effect of leakage aperture of high pressure carbon

٣٧٥   dioxide pipeline on Mach disk. The leak aperture affects the initial state of carbon dioxide

٣٧٦   outflow, with smaller apertures more likely to cause the flow velocity to reach supersonic

٣٧٧   speeds in order to form a Mach disk, and the location, strength, and stability of the disk varies

٣٧٨   with different apertures. In addition, the study helps to assess the extent of the hazard and

٣٧٩   predicts the rate and extent of CO_2 dispersion, which is essential for the identification of

٣٨٠   hazardous areas and the development of safety distances and emergency response strategies.

(1) Analysis of the impact of leakage hole diameter on the size of Mach disk

In order to deeply investigate the effect of leakage aperture on the size of the Mach disk, three experiments were carried out in this study: experiment I, experiment II and experiment III, and a detailed comparative analysis of the simulation results was carried out. The specific results can be seen in Fig. 10.

Simulation experiments show that the size of the Mach disk is positively correlated with the leak aperture, and the larger the leak aperture, the larger the Mach disk. This involves a number of hydrodynamic principles: First, the leakage aperture increases the flow rate increases, more gases pass through the leakage port at supersonic speeds, and a larger Mach disk is formed downstream; second, the leakage aperture change affects the surrounding pressure distribution, which in turn affects the generation and propagation of the excitation and expansion waves, and the interactions of these waves are significant for the generation of Mach disks; third, the expansion of the leakage aperture will enhance the degree of fluid turbulence and generate more vortices, which significantly affects the shape and size of the Mach disk, and according to the law of conservation of energy and momentum, the increase of the leakage aperture promotes the transfer of energy and momentum between the fluids, which affects the formation of Mach disk.

(2) Analysis of the influence of leakage aperture size on the formation time of Mach disk

In order to study in depth the extent to which the leakage aperture affects the time required for the formation of the Mach disk, the velocity clouds within 1 ms in Experiment I, within 5 ms in Experiment II, and within 10 ms in Experiment III were observed and analyzed in detail.

As illustrated in Figure 11, the time required for the formation of the Mach disk is positive correlated to the diameter of the leakage nozzle, i.e., a decrease in the diameter of the leakage nozzle corresponds to a decrease in the time required for the formation of the Mach disk. This phenomenon can be understood in terms of the time scale of fluid dynamics: a smaller orifice diameter means that the fluid passes through a narrower region, which in turn leads to a reduction in the time required. In addition, the formation of the excitation wave and its propagation speed increases with decreasing distance, facilitating the rapid formation of the Mach disk. The combination of accelerated compression and expansion of the fluid, shorter boundary layer development time, and more efficient energy transfer under smaller nozzle diameters contributes to the acceleration of the Mach disk formation process.

(3) Analysis of the impact of leakage aperture size on release rate

As shown in Figure 12, it can be observed that the velocity change curve has some general characteristics for all leakage calibres: the velocity curve goes through five stages of

development roughly. In the first stage, the velocity reaches the first peak at a certain growth rate. Subsequently, in the second stage, the velocity decreases rapidly to a trough value. In the third stage, the velocity rises from the trough to a smaller second peak and then decreases to an approximate size of the trough, forming a curve similar to the shape of a 'W'. In the fourth stage, the velocity rises from the trough to a third peak at a lower growth rate than in the first stage, which is lower than the initial peak. Finally, in the fifth stage, the velocity begins to decrease at a smaller rate.At the same time, there are some differences in the characteristics of the curves under different leakage apertures. When the leakage aperture is large, the "W" curve is farther away from the leakage port and more obvious. 4mm leakage aperture, the peak velocity is about 224m/s, and the minimum point is about 14mm away from the leakage port; 20mm and 40mm aperture, the peak velocity decreases to about 201m/s and 164m/s, respectively, and the minimum point increases to about 75mm and 142mm away from the leakage port. It can be seen that the smaller the leakage aperture is, the higher the peak velocity is after CO_2 leakage, and the closer the point of minimum velocity is to the leakage port.

From the above analysis, it can be inferred that the leakage velocity is negatively correlated with the leakage diameter. The smaller the diameter, the closer the minimum velocity point is to the leakage port. This is because in compressible flow, according to the area-velocity relationship, the effect of orifice contraction on flow velocity is related to the Mach number. At subsonic speeds, the flow velocity increases with a reduction in area, while at supersonic speeds, the opposite is true. A smaller leakage orifice will cause a more severe area contraction, resulting in a higher flow velocity gradient, making it easier for the fluid to reach the sonic velocity at the orifice throat, leading to choked flow. At this point, the mass flow rate is no longer affected by downstream pressure. Additionally, a smaller orifice diameter exacerbates the density drop during gas passage, further amplifying the flow velocity increment. When the throat reaches the sonic velocity and the downstream pressure is below a critical value, the gas expands freely outside the orifice, forming a Prandtl-Meyer expansion fan, which accelerates the flow velocity to supersonic speeds. In other words, a smaller orifice diameter promotes the formation of supersonic flow by enhancing the flow velocity gradient, inducing throat choked flow, and intensifying post-orifice expansion. The boundary layer at the small orifice leakage port is thinner, with a shorter development period and drastic velocity changes, making the minimum point closer to the leakage port. Furthermore, the interaction between shock waves and expansion waves at the small orifice is concentrated and limited in scope, also leading to the minimum velocity point being closer to the leakage port.

448   As shown in Fig. 12, due to the difference in the turbulence models used in the small and

449   large diameter leakage scenarios, the velocity cloud of the 4 mm diameter leakage simulation

450   with the k-ω turbulence model shows a significant bulge in the velocity recovery phase. In

451   contrast, the velocity maps of the 20 mm and 40 mm aperture leakage simulations with the k-

452   ε turbulence model show a smoother transition at the same stage.

453   *3.3.3 Effect of initial pressure on the temperature near the leakage port*

454   *(1) Analysis of the influence of initial pressure on near-field axial temperature*

455   When a high-pressure CO_2 pipeline leaks, the initial pressure affects its expansion degree

456   and temperature changes. Collect axial temperature data within 1 meter of the leakage port

457   after 8 ms of leakage in experiments five to seven and draw Fig. 13. The results indicate that

458   under different initial pressure conditions, the variation process of axial temperature with the

459   distance from the leakage port can be divided into four characteristic stages:firstly, when

460   leakage occurs, the CO_2 phase transition causes the temperature near the leakage port to drop

461   to the first trough value; Secondly, due to the Mach disk shock wave, the velocity decreased to

462   zero and the temperature slightly increased; Subsequently, due to the unstable velocity shock

463   wave behind the Mach disk, the temperature oscillation decreased to the second trough value;

464   After 8 ms of leakage, the temperature rose back to the experimental environment temperature

465   of 290 K. And the higher the initial pressure, the greater the cooling rate and amplitude. This

466   is because when high-pressure gas leaks, it expands, the internal energy decreases, and the

467   temperature decreases. The higher the pressure, the more energy is released, and the greater the

468   temperature drop; At the same time, high-pressure gas expands quickly, has strong heat

469   conduction and diffusion properties, exchanges heat quickly with the environment, and

470   promotes cooling.

471   (2) The influence of initial pressure on the near-field velocity Mach disk

472   To systematically explore the mechanism by which initial pressure affects the size of the

473   Mach disk, this study conducted three sets of control simulations, namely Experiment VII,

474   Experiment IX, and Experiment X, and performed a multidimensional quantitative analysis on

475   the results (refer to Figure 14 for details). The cloud chart data reveals that as the initial pressure

476   increases, the geometric dimensions of the Mach disk exhibit a significant expansion trend,

477   with a particularly pronounced increase in axial length. This is attributed to the fact that an

478   increase in initial pressure leads to a greater pressure difference between the jet stream and the

479   ambient gas, thereby intensifying the expansion of the jet stream at the outlet. According to the

480   shock wave polar line theory, an increase in pressure difference prolongs the process of shock

481 wave reflection and recompression, ultimately resulting in a significant increase in Mach disk

482 length. From the perspective of energy conservation, higher initial pressure imparts more

483 kinetic energy to the jet stream. When interacting with the ambient gas, this kinetic energy can

484 propel the shock wave front outward, ultimately manifesting as an increase in Mach disk size.

485 In stark contrast, the velocity peak in the core region of the Mach disk exhibits a step-like

486 decay. This is due to the fact that as the initial pressure increases, the jet undergoes more intense

487 shock compression and expansion cycles during its expansion process. This process results in

488 a significant conversion of kinetic energy into thermal and internal energy. Under the premise

489 of total energy conservation, an increase in pressure energy inevitably leads to a decrease in

490 kinetic energy (velocity). Furthermore, higher initial pressures trigger stronger viscous

491 dissipation and turbulence effects, further exacerbating the decay of the velocity peak.

492 *3.3.4 Simulation experiments in different leakage environments*

493 In the simulation of high-pressure CO_2 pipeline leakage, it is crucial to compare different

494 leakage environments, as high-pressure CO_2 leakage into water can trigger complex reactions.

495 It has high solubility in water and can change the phase distribution, which is significantly

496 different from leakage in air. Moreover, high concentrations of water-soluble CO_2 underwater

497 pose a risk of suffocation. In addition, due to its exothermic dissolution and high specific heat

498 capacity of water, it can also alleviate temperature changes and affect the dissolution and

499 diffusion of CO_2.

500 (1) Analysis of changes in CO_2 volume and velocity under different leakage environments

501 This study simulated a water leakage environment at a depth of 10 meters and conducted

502 experiments four and six to compare the velocity Mach disk, axial temperature changes, and

503 CO_2 volume generated by phase transition near the leakage point under different environments

504 after 10 seconds of leakage. The results of Experiment 4 and Experiment 6 are shown in Figure

505 15. After a leakage of 10ms, when high-pressure CO_2 leaks underwater, CO_2 accumulates at

506 the leakage port and diffusion is hindered due to various factors such as water solubility, density,

507 and viscosity. High solubility leads to the formation of a high concentration zone for CO_2, while

508 viscosity reduces diffusion rate. Changes in underwater pressure and temperature also promote

509 its accumulation.

510 In addition, as shown in Figure 15, when high-pressure CO_2 leaks underwater, the Mach

511 disk structure will be damaged. This is mainly because the speed of sound in water

512 ($c_{water} \approx 1480 m/s$) is approximately 4.3 times that in air ($c_{air} \approx 340 m/s$), significantly

٥١٣ reducing the Mach number ($M = \dfrac{V}{c}$) at the same jet velocity: $M_{water} = \dfrac{V}{1480} = M_{air} = \dfrac{V}{340}$.

٥١٤ Since shock waves are only formed at $M > 1$, the lower Mach number in water makes it

٥١٥ difficult for the CO_2 jet to maintain supersonic flow, disrupting the conditions for Mach disk

٥١٦ formation.

٥١٧   (2) Analysis of near-field axial temperature changes under different leakage environments

٥١٨   To investigate the effect of leakage environment on the near-field temperature,

٥١٩ Experiments IV and VI collected and plotted the axial temperature within 1 m of the leakage

٥٢٠ port and plotted a line graph 16 after 8 ms of leakage . The results indicate that after high-

٥٢١ pressure CO_2 leaks into water, the variation pattern of axial temperature with the distance from

٥٢٢ the leakage point exhibits significant similarity to the evolution trend of axial temperature in

٥٢٣ the atmospheric environment, but there are also differences:the first stage trough value is

٥٢٤ advanced to about 106 mm from the leakage port, and in the second stage, due to the rupture

٥٢٥ of the Mach disk, the temperature jumps over the the third stage directly back to 290 K. The

٥٢٦ experiments show that high pressure CO_2 leakage in water retards the low temperature diffusion

٥٢٧ more than in the atmosphere. This is due to the high thermal conductivity, density and viscosity

٥٢٨ of water, and the dissolved heat absorption of CO_2, which together slow down the low-

٥٢٩ temperature diffusion and reduce the leakage rate.

4. Conclusion

٥٣١   This article integrates the Peng-Robinson Equation of State (P-R EOS) and the Span-

٥٣٢ Wagner Equation of State (S-W EOS) for CO_2 physical property calculation. It predicts the

٥٣٣ near-field jet characteristics of high-pressure CO_2 pipeline leaks, analyzes the impact of leak

٥٣٤ diameter on the velocity Mach disk, the influence of initial pressure on near-field axial

٥٣٥ temperature and velocity Mach disk, as well as the effects of different leakage environments

٥٣٦ on the near-field leakage jet. Comparative analysis indicates that the k–ε turbulence model is

٥٣٧ more suitable for numerical simulation of large-diameter leakage scenarios, while the k-ω

٥٣٨ turbulence model is more applicable to small-diameter leakage scenarios.

٥٣٩   Due to the simplification of the formation process of dry ice solids in this study, it is not

٥٤٠ suitable for simulating the generation of dry ice. When the temperature is below 217 K,

٥٤١ significant deviations in simulation results will occur, making it only suitable for simulating

٥٤٢ near-field characteristics at temperatures above 217 K and within 10 ms after leakage. The

٥٤٣ formation mechanism of dry ice and its solutions require further research.

544

References

[1] Cai, W., Wang, G., Santoso, A. et al., "Increased frequency of extreme La Niña events under green house warming", *NAT CLIM CHANGE*, 5 (2), pp132-137 (2015). http://doi.org/10.1038/nclimate2492.

[2] Azar, C., Lindgren, K., Obersteiner, M. et al., "The feasibility of low CO2 concentration targets and the role of bio-energy with carbon capture and storage (BECS)", *CLIMATIC CHANGE*, 100 (1), pp195-202 (2010). http://doi.org/10.1007/s10584-010-9832-7.

[3] Onyebuchi, V. E., Kolios, A., Hanak, D. P. et al., "A systematic review of key challenges of CO2 transport via pipelines", *RNEW SUST ENERG REV*, 81 (2017). http://doi.org/10.1016/j.rser.2017.06.064.

[4] Blackford, J., Widdicombe, S., Lowe, D. et al., "Environmental risks and impacts of carbon dioxide (CO2) leakage in marine ecosystems" (2010). http://doi.org/10.1533/9781845699581.3.344.

[5] Liu, X., Godbole, A., Lu, C. et al., "Source strength and dispersion of CO2 releases from high pressure pipelines: CFD model using real gas equation of state", *APPL ENER*, 126, pp56-68 (2014). http://doi.org/10.1016/j.apenergy.2014.03.073.

[6] Zheng, W., Mahgerefteh, H., Brown, S. et al., "Integral Multiphase Turbulence Compressible Jet Expansion Model for Accidental Releases from Pressurized Containment", *Ind. Eng. Chem. Res.*, 55 (27), pp7558-7568 (2016). http://doi.org/10.1021/acs.iecr.6b01546.

[7] Schumann, D., "Public Perception of CO2 Pipelines", *Energy Procedia*, 114, pp7356-7366 (2017). http://doi.org/10.1016/j.egypro.2017.03.1867.

[8] Li, K., Zhou, X., Tu, R. et al., "Investigation of flow characteristics in small-scale highly pressurized leaked CO2 jet plume from pipeline", *Int. J. Therm. Sci.*, 141, pp160-170 (2019). http://doi.org/10.1016/j.ijthermalsci.2019.04.003.

[9] Teng, L., Liu, X., Bian, J. et al., "A homogeneous relaxation model for multi-phase CO2 jets following the release of supercritical CO2 pipelines ScienceDirect", *J Nat. Gas Sci. Eng.*, 84 (2020). http://doi.org/10.1016/j.jngse.2020.103609.

[10] Tian, G., Zhou, Y., Huang, Y. et al., "Experimental study of accidental release behavior of high pressurized CO2 vessel", *Process Saf. Environ. Prot.*, 145, pp83-93 (2021). http://doi.org/10.1016/j.psep.2020.07.051.

[11] Hu, Y., Yan, X., Chen, L. et al., "Leakage hazard distance of supercritical CO2 pipelines through experimental and numerical studies", *Int. J. Greenh. Gas Control*, 119 (2022). http://doi.org/10.1016/j.ijggc.2022.103730.

[12] Chen, J., Tang, X., Liu, Y. et al., "Exploration of the Impact of Supercritical CO2 Pipeline Fracture and Leakage", *Nat. Gas Oil*, 41 (2), pp1-8 (2023). http://doi.org/10.3969/j.issn.1006-5539.2023.02.001.

[13] Li Z. "Research on Safety Characteristics of High Pressure Carbon Dioxide Pipeline under Complex Conditions", *Shijiazhuang Tiedao University* (2023). http://doi.org/10.27334/d.cnki.gstdz.2023.000342.

[14] Zhang Z., Liu Z., Yan L. et al. "Experiment and numerical investigation on flow characteristics and near field structure of dense phase CO2 pipeline leakage", *PROCESS SAF ENVIRON*, 182 (2024). http://doi.org/10.1016/j.psep.2023.11.084.

[15] Wang J., Li H., Feng H. et al. "Consequence of high pressure CO2 pipeline failure Full scale burst test and numerical simulation", *J Loss Prev. Process Ind.*, 9 (2024). http://doi.org/10.1016/j.jlp.2024.105489.

[16] Sun J. "Analysis and Study of Supercritical Dense Phase CO2 Leakage Process in CCUS Pipeline", *Energy Sav. Meter. Pet. Petrochem. Ind.* (12) (2024). http://doi.org/10.3969/j.issn.2095-1493.2024.12.014.

[17] Liu Z., Wu P., Wen H. et al. "Effect of source strength on the simulation of jet dispersion and hazard distances during accidental release of liquid CO2", *Process Saf. Environ. Prot.*, 183, pp. 1152-1169 (2024). http://doi.org/10.1016/j.psep.2024.01.064.

[18] Shang Y., Chen X., Wu P. et al. "A new model for predicting characteristics of the near field leakage in high pressure CO2 pipelines", *J Pipeline Sci. Eng.*, 5 (2025). http://doi.org/10.1016/j.jpse.2024.100249.

[19] Wang J., Yan L., Xiao C. et al. "Experimental study of near field characteristics of high pressure CO2 pipeline leakage", *Int. J. Greenh. Gas Control*, 37 (2024). http://doi.org/10.1016/j.ijggc.2024.104205.

[20] Sun Y., Chen X., Zhou S. et al. "Research on Leakage and Diffusion Behavior of Underwater Gas Pipeline", *J Changzhou Univ. (Nat. Sci. Edn.)*, (2), pp. 52-61 (2025). https://link.cnki.net/urlid/32.1822.N.20241231.0957.002

[21] Ansys CFX Solver theory guide, Ansys Inc. 2023 (2023).

[22] Lee W. H. "PRESSURE ITERATION SCHEME FOR TWO PHASE FLOW MODELING", Computational Methods for Two Phase Flow and Particle Transport With DRM (())

[23] Peng D. Y., Robinson D. B. "A New Two Constant Equation of State", *Ind. Eng. Chem. Fundam.*, 15, pp. 59-64 (1976). http://doi.org/10.1021/i160057a011.

[24] Flechas T., Delphine M. G., Glover C., Charles I. "A 2D CFD model for the decompression of carbon dioxide pipelines using the Peng Robinson and the Span Wagner equation of state", *PROCESS SAF ENVIRON*, 140 (2020). http://doi.org/10.1016/j.psep.2020.04.033.

[25] Span R., Wagner W. "A New Equation of State for Carbon Dioxide Covering the Fluid Region from the Triple Point Temperature to 1100 K at Pressures up to 800 MPa", *J Phys. Chem. Ref. Data*, 25, pp. 1509-1596 (1996). http://doi.org/10.1063/1.555991.

[26] Pursell M. "Experimental investigation of high pressure liquid CO2 release behaviour" (2012)

[27] Wareing C. J., Woolley R. M., Fairweather M. et al. "Numerical Modelling of Turbulent Particle laden Sonic CO2 Jets with Experimental Validation", *Procedia Eng*, 102, pp. 1621-1629 (2015). http://doi.org/10.1016/j.proeng.2015.01.298.

Table 1 Comparison of near-field Mach disks for high-pressure CO₂ pipeline leakage with different turbulence models

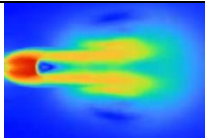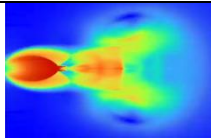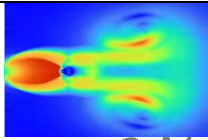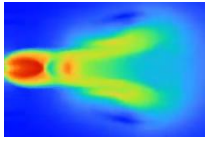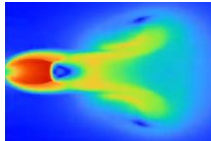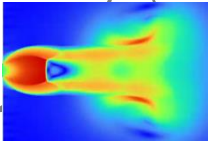| turbulence model	leak aperture		
	4mm	20mm	40mm
k-w model			
k-ε model			

Table 2 Numerical simulation of experimental conditions

Numerical simulation of experimental conditions						
Experiment number	Initial pressure (MPa)	Initial temperature (K)	Leakage aperture (mm)	Leak environment	Leakage ambient pressure (Pa)	Leakage ambient temperature (K)
I	4.05	269.65	4	Atmospheric	101325	290
II	4.05	269.65	20	Atmospheric	101325	290
III	4.05	269.65	40	Atmospheric	101325	290
IV	12	280	40	underwater	101325	290
V	9	280	40	Atmospheric	101325	290
VI	12	280	40	Atmospheric	101325	290
VII	15	280	40	Atmospheric	101325	290
VIII	6.89	280	1	Atmospheric	101325	290
IX	6	280	40	Atmospheric	101325	290
X	18	280	40	Atmospheric	101325	290
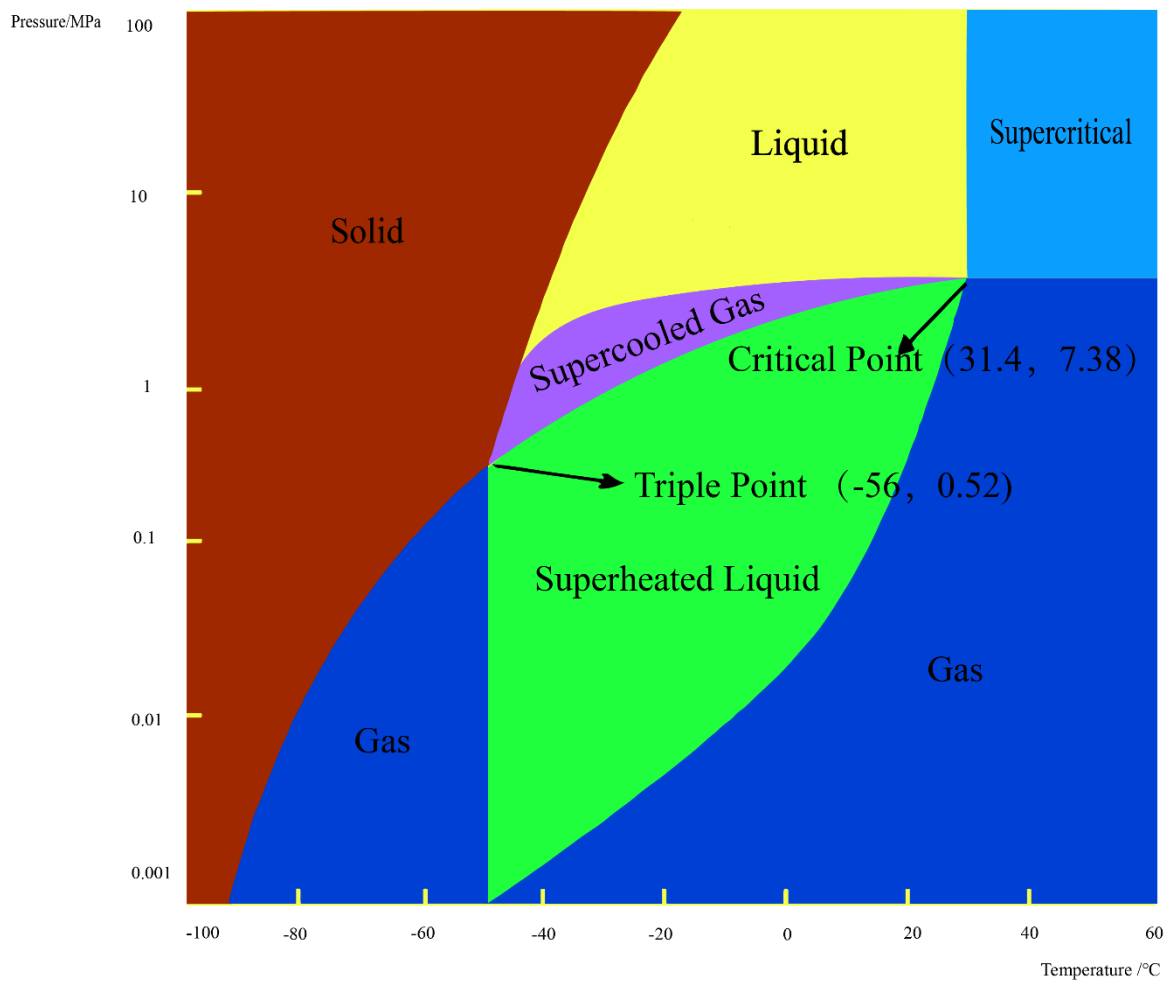
Fig.1 Phase diagram of CO$_2$
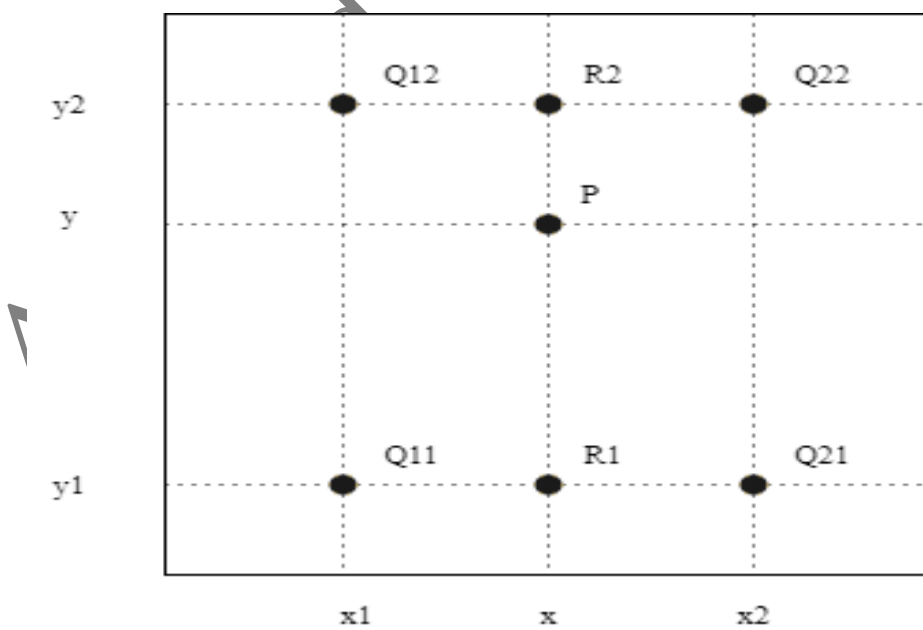
Fig.2 Schematic diagram of bilinear interpolation principle
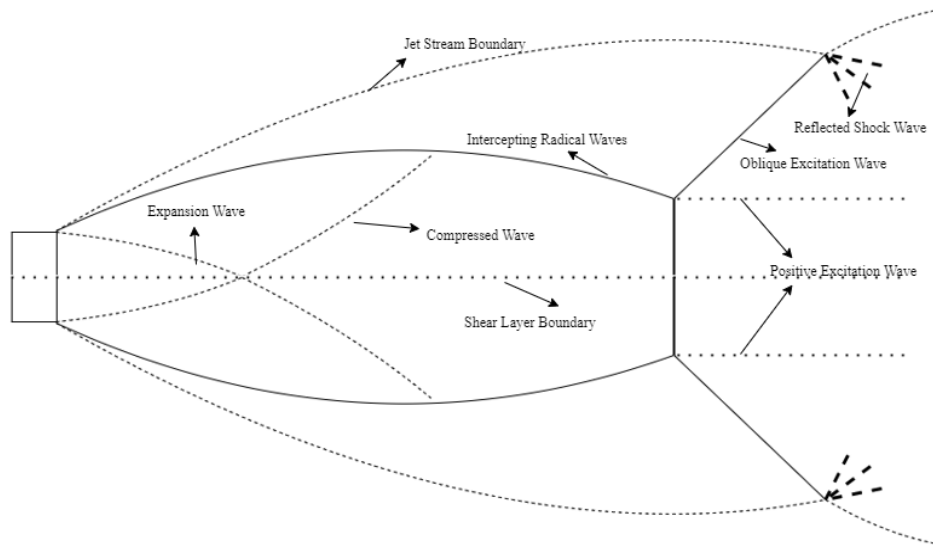
Fig.3 Schematic diagram of Mach disk structure
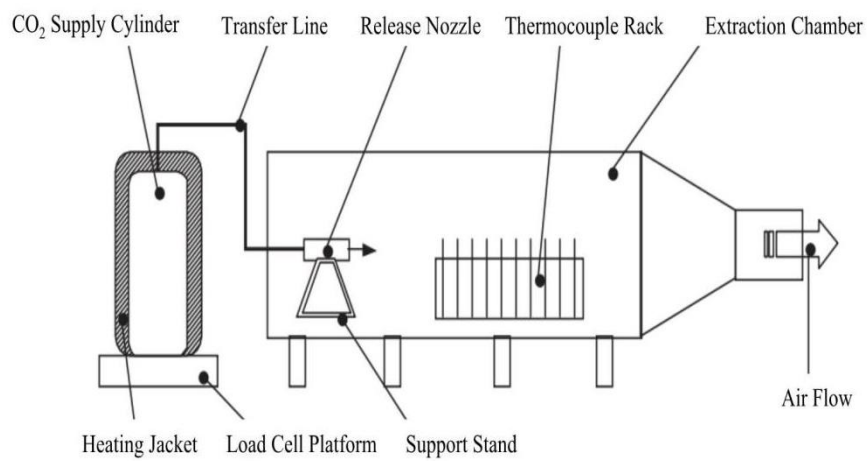
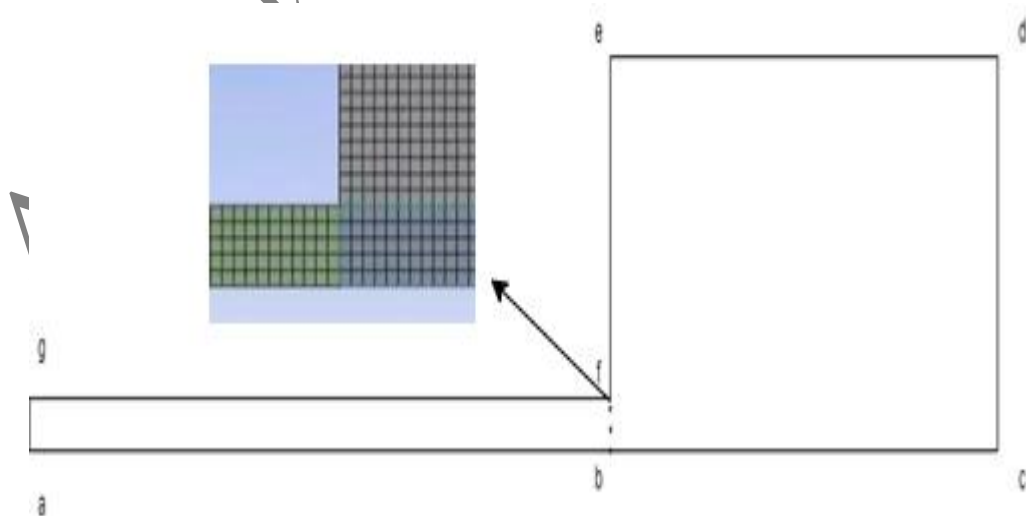**Fig. 4 Schematic diagram of the experimental setup**
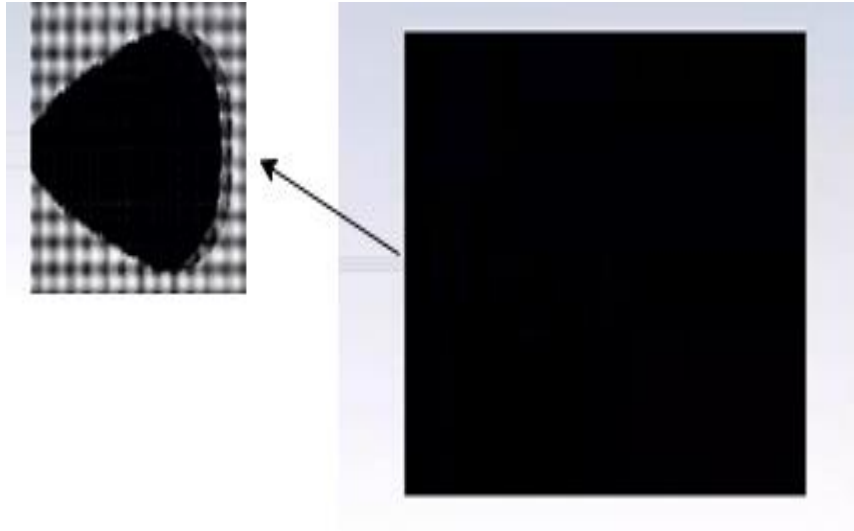
Fig. 5 Schematic of model and mesh.

٦٤٥

٦٤٦

٦٤٧   **Fig.6: The adaptive grid automatically performs the refinement process and marks**

٦٤٨   **the leakage area after the phase transition occurs**

٦٤٩
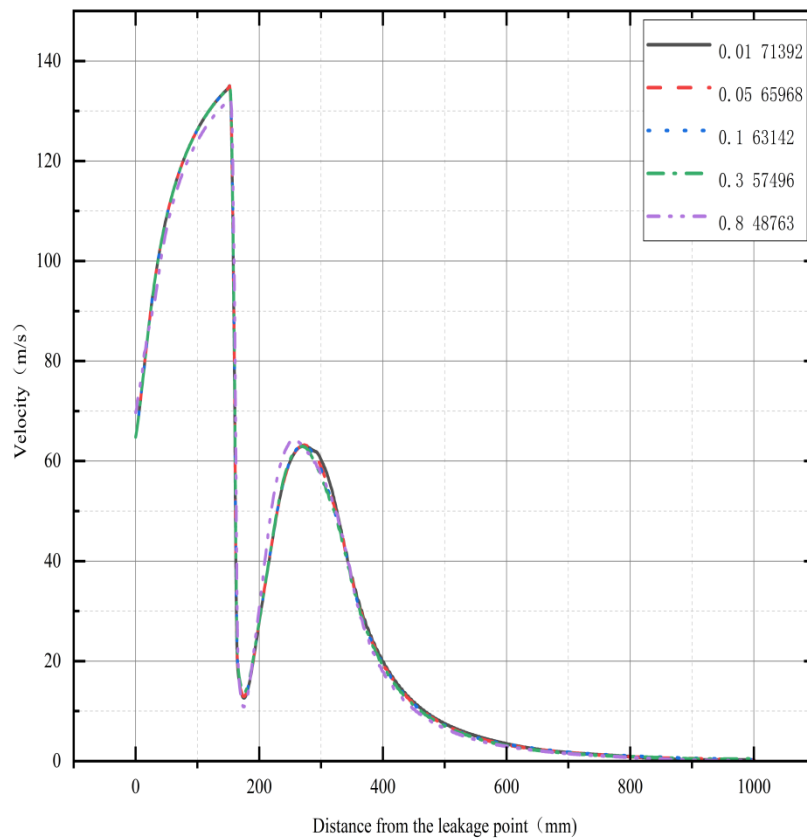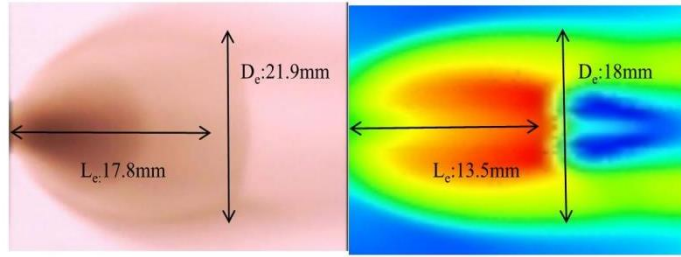
٦٥٠   **Fig.7 Grid Independence Verification**

Note: D_e:21.9mm, L_e:17.8mm (left); D_e:18mm, L_e:13.5mm (right)

٦٥١

٦٥٢ **Fig. 8 Comparative analysis of experimental and numerical simulation results**

٦٥٣
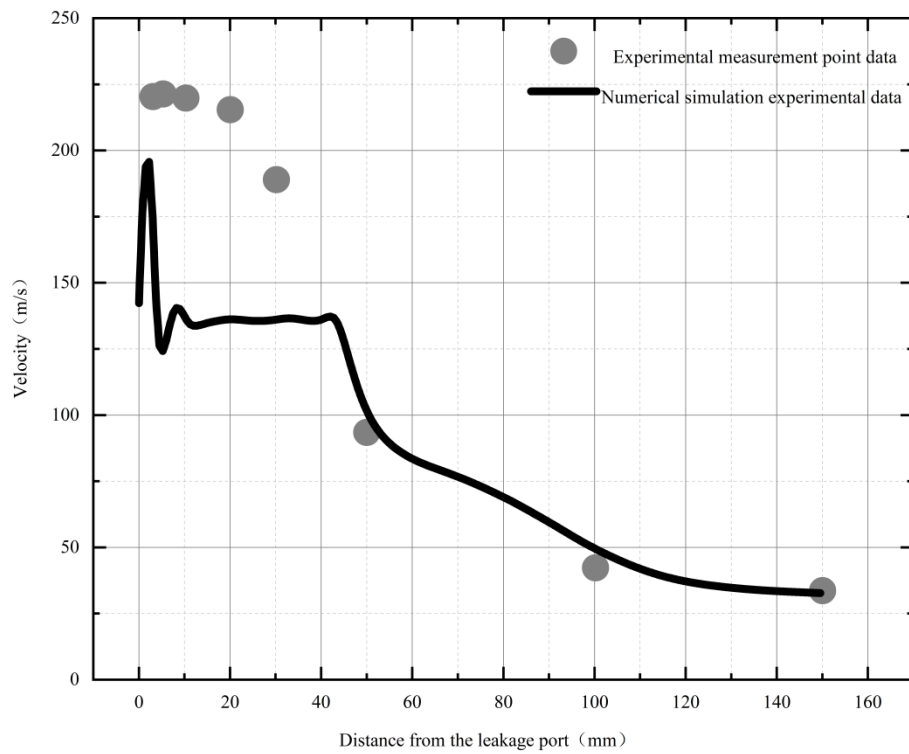
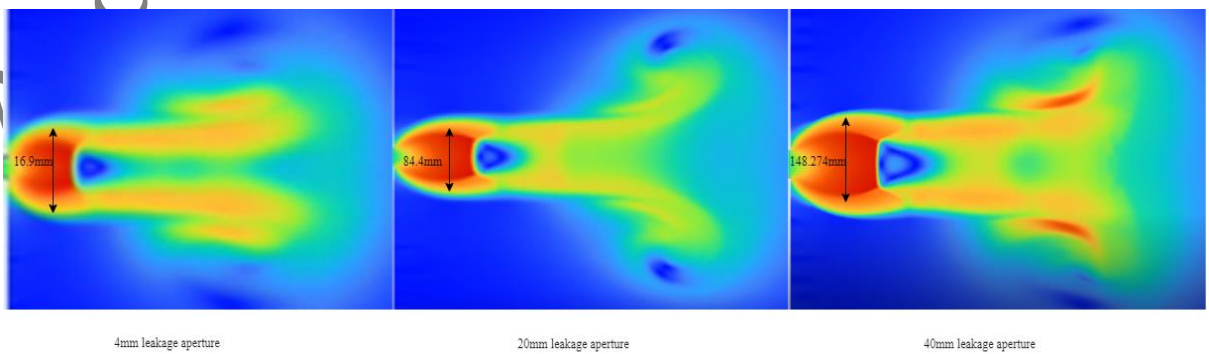٦٥٤ **Fig.9 Comparative analysis of experimental and numerical simulation results**

٦٥٥

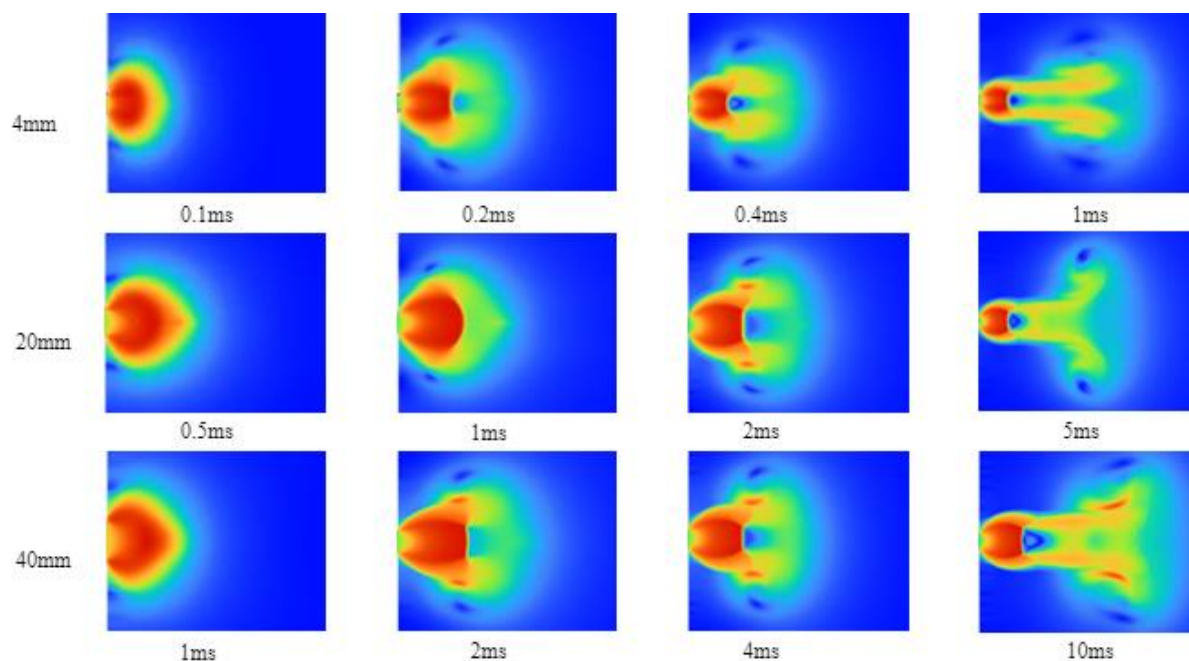٦٥٦ **Fig.10. Mach disc size cloud for different leakage apertures.**

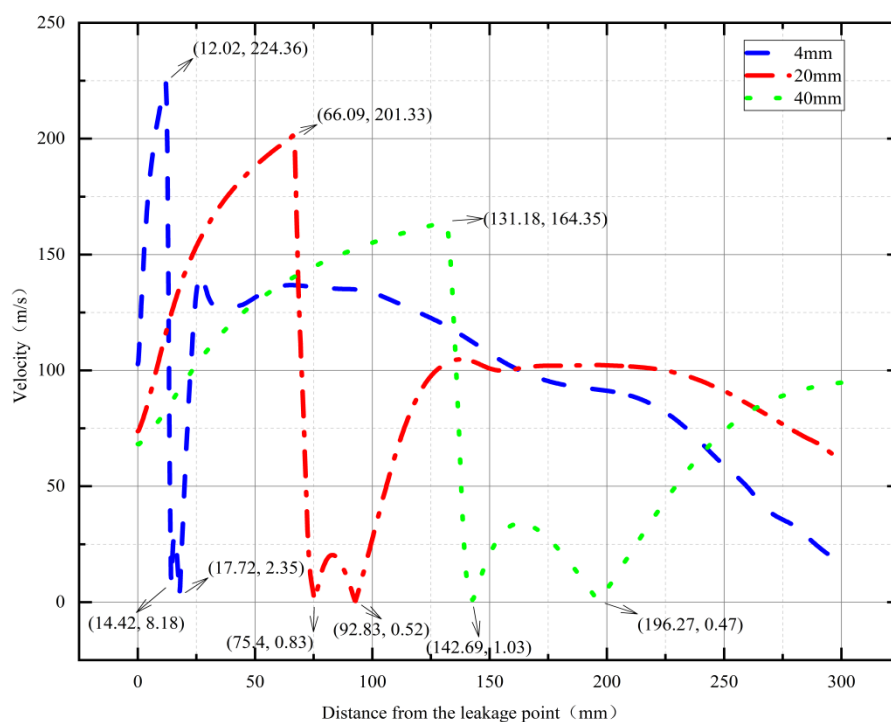**Fig.11 Velocity variation cloud for different leakage aperture**

Fig.12 Axial velocities within 0.3m from the leakage port after 5ms of leakage for
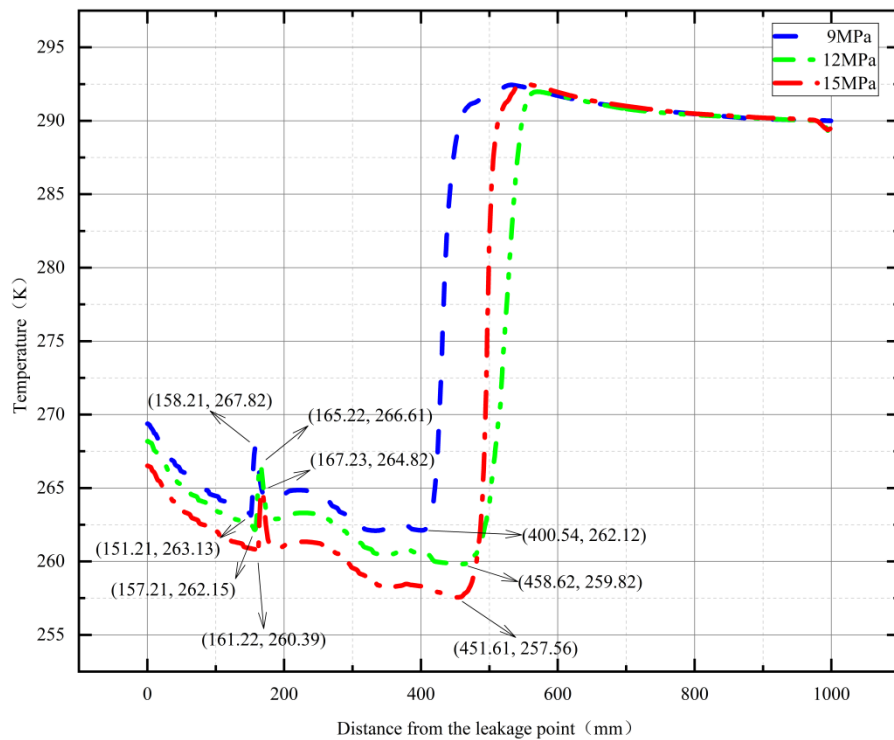
different leakage apertures

٦٦٢

Fig.13Axial temperature within 1m of the leakage port after 8ms of leakage at
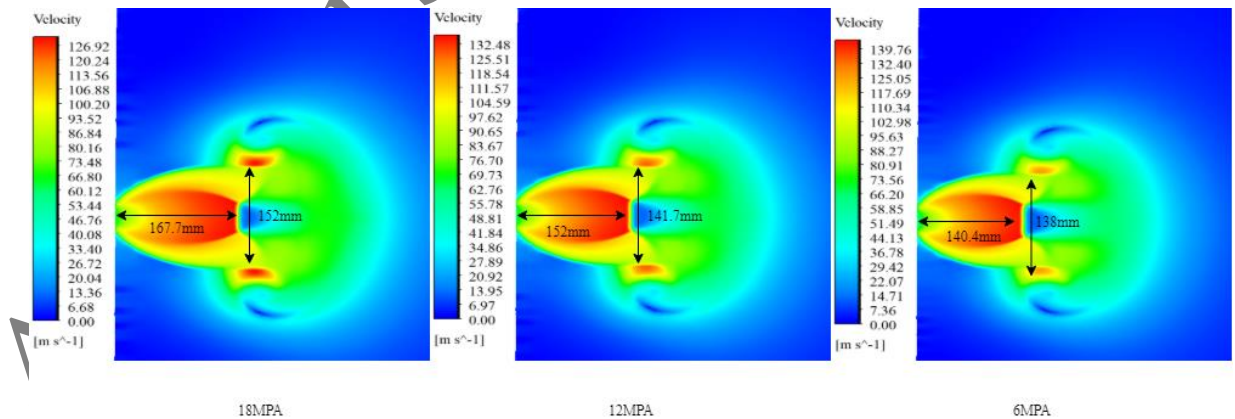
٦٦٣

different initial pressures

٦٦٤

٦٦٥

٦٦٦

18MPA   12MPA   6MPA

٦٦٧

Fig.14 Velocity contour map after 5ms of leakage under different initial pressures

Volume cloud of CO$_2$ after phase transition of CO$_2$ leaking into water

Volume cloud of CO$_2$ after phase transition of CO$_2$ leaking into the atmosphere

Velocity cloud of CO$_2$ leakage into water

Velocity cloud of CO$_2$ leakage into the atmosphere

2ms   4ms   8ms

٦٦٨
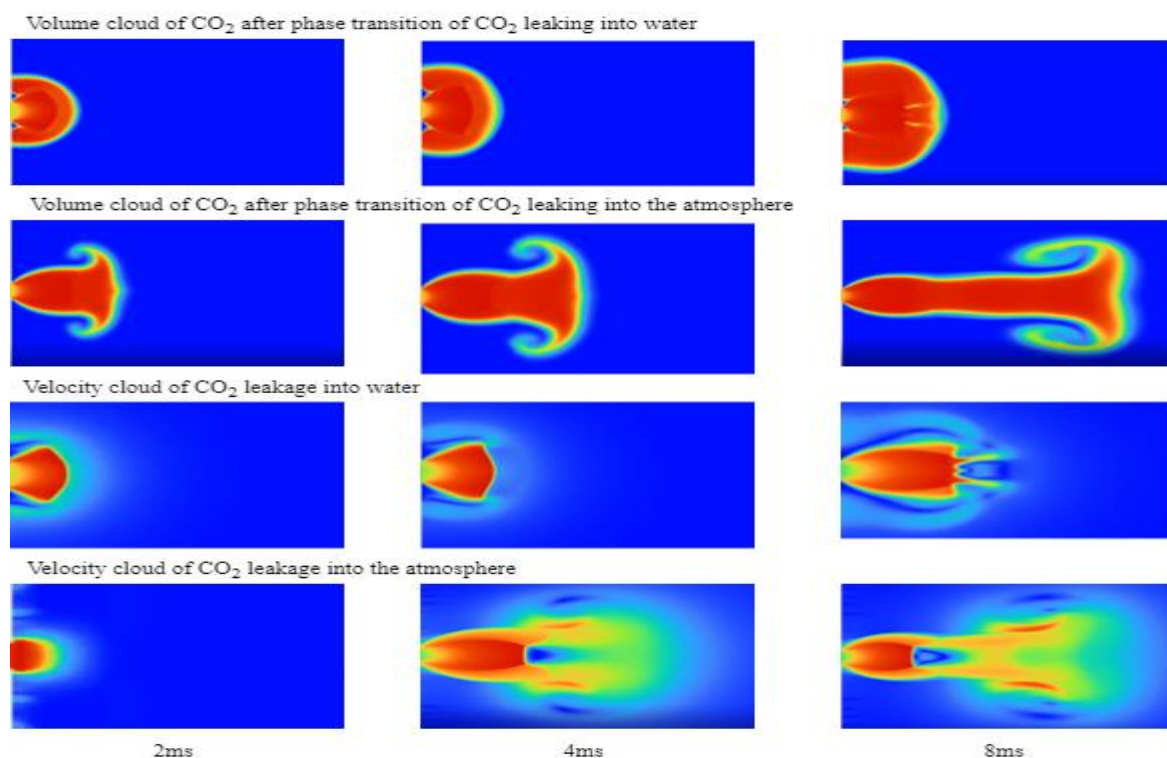
٦٦٩   **Fig.15Velocity cloud and CO$_2$ volume cloud after 10 ms of leakage in different**

٦٧٠   **leakage environments**
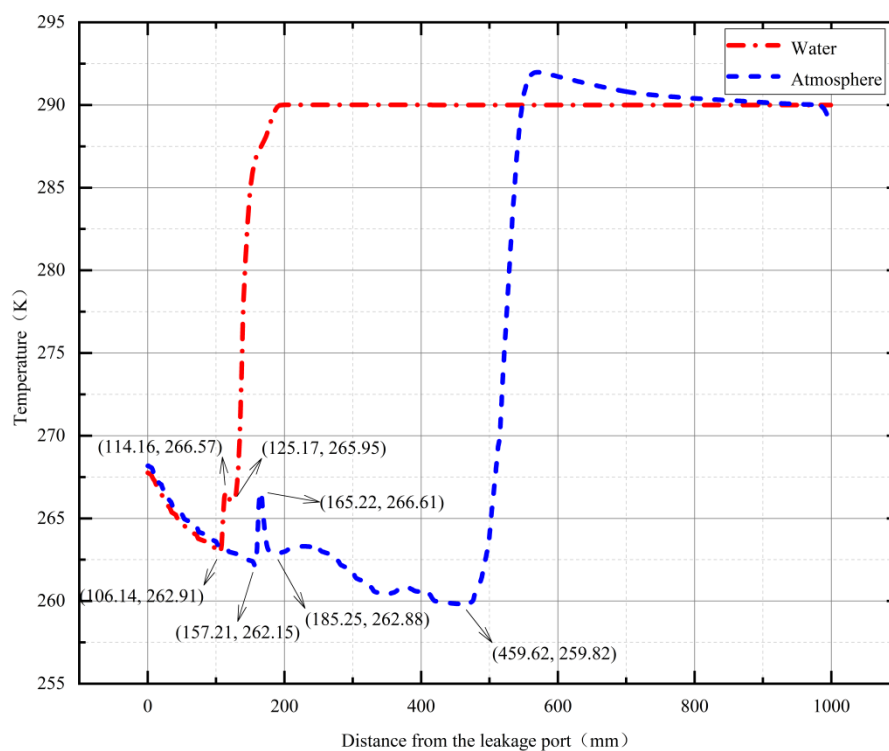
٦٧١

٦٧٢

٦٧٣   **Fig. 16 Axial temperature within 1m of the leakage port after 8ms of leakage in**

٦٧٤   **different leakage environments**

٦٧٥   Fujia Liu born in Shanxi in April 1998, is currently pursuing a master's

٦٧٦   degree in Petroleum and Natural Gas Engineering at Liaoning Shihua

٦٧٧   University. He obtained his bachelor's degree in Electronic Information

٦٧٨   Engineering from Shanghai Polytechnic University.

٦٧٩   Professionally, he has interdisciplinary knowledge and is proficient in core

٦٨٠   technologies such as Keil5 software development, AD circuit design, and Fluent

٦٨١   fluid simulation. He holds certificates including CET-6 and Junior Simulation

٦٨٢   (CAE) Application Engineer. He has participated in research projects like the

٦٨٣   design of an ECG disease identification system based on Arduino. In the

٦٨٤   analysis of leakage characteristics of high-pressure CO_2 pipelines, he used

٦٨٥   FLUENT to establish a real gas model and realized gas-liquid transition

٦٨٦   simulation through UDF programming, with relevant research having certain

٦٨٧   reference value for the CCUS field.

٦٨٨

٦٨٩   Ting Li is studying for amaster's degree in oil and gas storage and

٦٩٠   transportation engineeringat Liaoning Petrochemical University. He is interested

٦٩١   in the safe, economical, and environmentally friendly transportation technology

٦٩٢   of easy condensate and high-viscosity crude oil.

٦٩٣

٦٩٤   Yuguo Wu, male, Professor, Doctor, Supervisor of Master's Students. He is

٦٩٥   an Innovative Talent of Liaoning Provincial Higher Education Institutions and a

٦٩٦   member of the Oil and Gas Storage and Transportation Sub-technical

٦٩٧   Committee of the National Standardization Technical Committee for Petroleum

٦٩٨   and Natural Gas. His main research directions include safe and economic

٦٩٩   operation of oil and gas pipelines, safety technology for oil and gas storage and

٧٠٠   transportation facilities, and research on the construction and application

٧٠١   platform of standards related to oil and gas storage and transportation. He has

٧٠٢   long been engaged in the research of oil and gas storage and transportation

٧٠٣   technology. In recent years, he has published more than 100 academic papers,

٧٠٤ won 1 first prize each for provincial scientific and technological progress award

٧٠٥ and literary award, presided over 4 provincial and ministerial projects, and

٧٠٦ undertaken more than 30 industry and enterprise projects.

٧٠٧

٧٠٨   Xiaoling Li , female, Associate Professor, Doctor, Supervisor of Master's

٧٠٩ Students. Her main research directions include natural gas transportation

٧١٠ technology and urban gas transmission and distribution technology. In recent

٧١١ years, she has presided over 2 provincial-level projects and 6 horizontal projects

٧١٢ from enterprises, and published 4 SCI papers.

٧١٣

٧١٤

٧١٥